Enhanced H_2O_2 production over Au-rich bimetallic Au-Pd nanoparticles on ordered mesoporous carbons.

Tomás García*[a], Said Agouram [b], Ana Dejoz [c], Juan F. Sánchez-Royo[d], Laura Torrente-Murciano [e], Benjamín Solsona *[c]

[a] *Instituto de Carboquímica, ICB-CSIC, Zaragoza, Spain*
[b] *Department of Applied Physics and Electromagnetism, Universitat de Valencia, Valencia, Spain*
[c] *Department of Chemical Engineering, Universitat de Valencia, Valencia, Spain*
[d] *ICMUV, Universitat de València, Valencia, Spain*
[e] *Department of Chemical Engineering, University of Bath, Bath, BA2 7AY, UK*

Abstract

The industrial implementation of hydrogen peroxide as a green oxidant requires the development of efficient catalytic systems for its direct synthesis from molecular oxygen and hydrogen. Bimetallic Au-Pd nanoparticles supported on acid pre-treated ordered CMK-3 carbon catalysts show high H_2O_2 productivities and high H_2 selectivities (>99%). Encapsulation of the nanoparticles within the pore network lead to stable small size (~2 nm) particles. This paper reveals that the acid pre-treatment, does not only improve the metal dispersion of metals but most importantly, it promotes their gold enrichment, dramatically decreasing the parallel H_2O_2 decomposition, which is key for the economic feasibility of the process.

Keywords: hydrogen peroxide; direct synthesis; AuPd alloys; nanoparticles; acid treatment, CMK-3, ordered carbon.

1. Introduction

* Corresponding authors: Tomás García, ICB-CSIC, C/Miguel Luesma Castán, 50018 Zaragoza (Spain), Fax: (+34) 976733977, E-mail: tomas@icb.csic.es
Benjamín Solsona, Dept. Chemical Engineering, Universitat de Valencia. Avda. Universitat, 46100 Burjassot (Spain), Fax: (+34) 963544898, **E-mail: benjamin.solsona@uv.es

Since the onset of green chemistry in the early 90s, great scientific effort has been made towards the implementation of cleaner oxidants as an alternative to the industrially-used stoichiometric ones, in order to reduce the production of waste and energy consumption. Particularly, hydrogen peroxide (H_2O_2) is an efficient oxidising agent with a highly active oxygen content that produces only water as a co-product, however, its current large scale synthesis via the anthraquinone autoxidation route produces large quantities of waste with a high environmental impact [1, 2]. In contrast, the direct synthesis of hydrogen peroxide from molecular hydrogen and oxygen offers the possibility of obtaining hydrogen peroxide through a very clean reaction, with low operating costs, as only water is obtained as a by-product [3,4].

Nowadays, the most efficient catalysts for the direct synthesis are based on palladium [5-7]. Different preparation methods, additives, supports and reaction conditions have been studied to maximise the productivity and hydrogen utilisation of the reaction [8-12]. The catalytic performance of palladium-based catalysts can be improved when palladium is alloyed with a second metal, especially gold [13-16]. Based on theoretic calculation, gold-based catalysts present a higher potential for hydrogen peroxide formation than palladium [17], however, in practice, only-gold catalysts hardly yield hydrogen peroxide [18]. Thus, although the role of gold is not evident, its contribution to the enhanced performance of the bimetallic AuPd catalysts is extremely important and it has been related to several factors [19, 20] mainly *i.* the presence of gold improves the dispersion of palladium, *ii.* the formation of highly dispersed bimetallic AuPd particles tends to decrease the decomposition of the hydrogen peroxide formed, *iii.* the ability of Au to form hydroperoxy species, a precursor of hydrogen peroxide and *iv.* gold causes an electronic modification of the Pd surface.

The selection of the catalytic support has been demonstrated to be of paramount importance as it determines the metal dispersion and the interaction with the metal. As an example, in the case of gold-based systems, inert supports such as activated carbon and siliceous materials yield high concentrations of hydrogen peroxide, in contrast with other acidic and basic supports, which are inefficient for this reaction [21]. On the other hand, in the case of bimetallic AuPd catalysts, acidic supports such as TiO_2 have been reported to be more efficient for AuPd than others such as iron oxide, alumina and cerium oxide [22-24]. Additionally, the surface properties of the support can be modified to tune the final reactivity of the catalytic system. Specifically, pre-treatment of the support using nitric acid has been demonstrated to be beneficial in the direct synthesis of hydrogen peroxide [25-27]. In AuPd bimetallic systems, the acid treatment of carbon supports increases the hydrogen peroxide formation as it decreases the amount of active sites for nonselective hydrogenation due to an improvement in the dispersion of the Au-Pd alloy particles [25]. Using titania as a support for AuPd, the formation rate of hydrogen peroxide also increases with acid pre-treatments but in this case, the switch-off of the sequential H_2O_2 hydrogenation/decomposition reaction does not take place. In this case, the enhanced hydrogen peroxide formation is linked to an improvement of the dispersion of gold within the catalyst, leading to an increased proportion of smaller Au–Pd-nanoparticles, [26].

Following the work by Ryoo *et al.* [28] related to the high dispersion of platinum nanoparticles on ordered carbon supports compared to other carbonaceous materials, we have recently communicated the use of CMK-3 carbon as a support for AuPd nanoparticles [27]. High productivity values towards the direct synthesis of hydrogen peroxide were obtained when the ordered support was pre-treated with nitric acid. This paper further explores the reasons behind such an increase in reactivity related not only

to the high dispersion of small (2-3 nm) bimetallic nanoparticles, but most importantly, their high gold content (Au/Pd: 56/44), with very low activity towards the subsequent hydrogen peroxide decomposition.

2. Experimental

2.1. Synthesis of catalysts

Ordered carbon with a CMK-3 structure was synthesised by impregnating SBA-15 mesoporous silica at 30ºC with a furfuryl alcohol solution containing oxalic acid, followed by treatment in helium at 300ºC for 1 h and at 850ºC for 4 h. The resulting powder was leached with concentrated sodium hydroxide to remove the silica template and washed three times with plenty of deionized water and acetone. The final CMK-3 carbon was dried in air at 90ºC. Non-ordered mesoporous activated carbon supplied by NORIT was also used for comparison.

Both carbons (ordered and non-ordered) were used as supports either untreated or pre-treated with nitric acid as described elsewhere [29]. Overall, four different carbon supports were employed: ordered/treated, ordered/untreated, non-ordered/treated, non-ordered/untreated.

Gold, palladium and gold/palladium catalysts were synthesised by incipient wetness impregnation of the four different carbon supports with an aqueous metal solution. The slurry was then stirred and evaporated at 80ºC. Palladium chloride ($PdCl_2$) and gold chloride ($HAuCl_4 \cdot 3H_2O$) from Sigma Aldrich were used as metal precursors without any prior purification.

2.2 Characterisation techniques

Activated carbon supports and catalysts were characterised by N_2 adsorption at -196ºC using a Micromeritics ASAP 2020 apparatus after degasification at 150ºC. The surface area (S_{BET}) was estimated by the Brunauer-Emmet-Teller (BET) method using multipoint data from the relative pressure range of 0.05-0.25. Mesopore volumes and pore size distributions were calculated using the Barrett-Joyner-Halenda (BJH) method, applied to the desorption branch of the N_2 adsorption isotherm.

Calcination experiments were carried out in a fixed bed reactor coupled to a mass spectrometer (Thermostar, Balzers) to characterise the surface chemistry of all the catalysts. In these experiments, 100 mg of sample were heated up to 950°C under an Argon flow rate of 50 ml/min.

CO chemisorption analyses were carried out in an AutoChem II instrument from Micromeritics equipped with a TCD. Prior to the analysis, samples were pre-treated under helium at 300°C to remove any adsorbed molecules from the surface. Then, the samples were treated under a 5%CO/He flow for 1 hour at 25ºC followed by a flow of helium for 15 minutes to remove any physisorb CO. The amount of chemisorb CO was recorded from room temperature to 300 ºC with a carrier flow of He of 10 mL/min by using a programmed rate of 10ºC/min.

X-ray photoemission (XPS) measurements were performed in an ESCALAB 210 multianalysis system (base pressure 1.0×10−10 mbar) from Thermo VG Scientific. Photoelectrons were excited with the MgKα line. The hemispheric photoelectron analyser worked with a pass-energy of 20 eV. The charge process of the sample during the XPS measurements was discarded by ensuring that the C1s core level peak was assigned at 284.5 eV.

Powder X-ray diffraction was used to identify the crystalline phases present in the catalysts. An Enraf Nonius FR590 sealed tube diffractometer, with a monochromatic CuKα1 source operated at 40 kV and 30mA was used. XRD patterns were calibrated against a silicon standard and phases were identified by matching experimental patterns to the JCPDS powder diffraction file.

Metal particle size distribution was determined by high resolution Transmission Electron Microscopy (HR-TEM). For each sample, over 100 particles from different parts of the grid were used to estimate the mean diameter and size distribution of particles. The samples were also used to determine the elemental composition of particles by EDX, EDX-mapping analysis using a Field Emission Gun (FEG) TECNAI G2 F20 operated at 200 kV and selected area electron diffraction (SAED).

2.3 Catalytic tests

The synthesis of the hydrogen peroxide reactions were carried out in a 250 mL stainless steel autoclave reactor loaded with solvent (75 ml of methanol, 0.04M HCl) and catalyst (75 mg). The reactor was then purged with hydrogen three times. Once the temperature (5ºC) was stable, the autoclave was filled with a mixture of H_2/O_2/Ar (5/10/85 %) at 20 bar of pressure. To ensure an appropriate mixture, a four propeller stirrer was used at 1000 rpm. The hydrogen peroxide concentration was determined by titration with cerium sulphate. After reactions, the gas phase was analysed by gas chromatography in order to determine hydrogen selectivity. No conversion was obtained in the absence of the catalyst.

The decomposition of the hydrogen peroxide reactions were conducted in a glass reactor containing 60 ml of a 1.6 M aqueous solution of H_2O_2 and 50 mg of catalysts at

atmospheric pressure and a reaction temperature of 5ºC. The decomposition reaction was followed by analysing the hydrogen peroxide concentration periodically by titration of samples with cerium sulphate.

3. Results and discussion

Table 1 summarises the four carbon supports used in this study. All supports show negligible activity towards hydrogen peroxide direct synthesis (<0.1 mmol/L after 1h of reaction) independently, if they are ordered or non-ordered, untreated or acid-treated. In contrast, gold, palladium and gold-palladium catalysts supported on activated carbon show substantial formation of hydrogen peroxide, confirming that the activity is due to the presence of metal active species. Table 2 shows the different catalysts synthesised, their nomenclature and physical properties.

Catalytic results towards the direct synthesis of hydrogen peroxide of monometallic Au, monometallic Pd and bimetallic AuPd catalysts supported on acid-treated and untreated ordered mesoporous carbons are shown in Table 3. Results obtained for non-ordered commercial activated carbons as supports are also included for comparative purposes. For ordered carbons, it is observed that H_2O_2 yields after 60 min by the gold-only catalysts (either AO or AO20) are significantly lower (*ca.* 4 mmol/L after 1h) than those of the palladium–only catalysts (either PO or PO20). The significant difference of activities of the monometallic gold and palladium catalysts is mainly caused by the intrinsic reactivity of both metals, being the disparity of metal particle sizes in both catalysts, as shown later, a possible additional factor. Moreover, it can be observed in Table 3 that bimetallic AuPd catalysts lead to remarkable higher hydrogen peroxide

formation compared to the corresponding monometallic catalysts. For example, the bimetallic gold-palladium catalyst (APO20) supported on the acid-treated ordered carbon shows a productivity *ca.* 50% and 650% higher than the corresponding monometallic palladium (PO20) and gold (AO20) catalysts, respectively. In fact, it can be seen that there is a synergetic effect between both metals after alloy formation. Similar effect is observed for the catalyst supported on the untreated ordered carbons. Remarkably, the use of an ordered carbon (CMK-3) as a support for AuPd nanoparticles, results in more efficiency in the formation of hydrogen peroxide than the mesoporous NORIT non-ordered commercial carbon (either acid-treated or untreated). In addition, it should be mentioned that an important enhancement in the productivity is achieved by the acid treatment of the support prior to metal loading. The bimetallic catalyst supported on the acid-treated ordered carbon (APO20) resulted in the most efficient catalyst with a notable productivity of H_2O_2 (32 mmol/L after 1 h), two fold higher than that obtained in the case of AuPd catalysts supported on untreated carbon (APO, 15 mmol/L after 1 hour). As for the lab-made ordered carbons, an improvement of the hydrogen peroxide production is also observed for the bimetallic catalyst supported on the acid-treated commercial carbon, since the H_2O_2 productivity in 1 hour is increased from 11 mmol/L to 19 mmol/L. Finally, it should be pointed out that although acid treatment does not exert any influence on the catalytic activity of gold monometallic catalyst, a positive effect is observed in the case of either palladium or bimetallic catalysts regardless of the nature of the carbon support, mainly related to the presence of smaller nanoparticles.

Table 3 also shows that the presence of gold in the small bimetallic nanoparticles is directly related to the suppression of the subsequent hydrogen peroxide decomposition

during the synthesis reactions. Accordingly, Figure 1a compares the evolution of the concentration of hydrogen peroxide during the reaction with respect to time using the AuPd catalysts. It can be observed that, the nitric acid pre-treatment of the support seems to be critical in order to achieve high productivities as it prevents the hydrogen peroxide decomposition at long reaction times. This effect is clearly apparent after 10 min of reaction, as the concentration of H_2O_2 formed by the AuPd catalyst supported on untreated carbon decreases, whereas the productivity increases in those supported on acid-treated carbons (AP20 and APO20). Thus for the untreated bimetallic catalyst the concentration after 10 min is 11 mmol/L and after 90 min it has decreased *ca.* 50% until 5.6 mmol/L. Similarly for the APO catalyst, the concentration after 10 min is 18 mmol/L whereas after 90 min it has decreased to 11 mmol/L. In contrast to AP20 and APO20, the concentrations after 10 min are 13 and 27 mmol/L but after 90 min, these values are increased to 19 and 36 mmol/L respectively. This decrease of hydrogen peroxide concentration is obviously directly related to the hydrogen selectivity of the process, which is key to the economic feasibility at industrial scale. In fact, a high hydrogen selectivity >99% is observed for the APO20 catalyst, which decreases to 89% for the non-ordered counterpart catalyst (AP20). As previously reported [33], acid pre-treatment can promote the formation of gold-rich bimetallic particles which suppress the O-O bond scission in the decomposition reaction.

Additionally, the decomposition of H_2O_2 was studied independently from its direct synthesis. All the metal-free carbon supports used in this study (ordered/non-ordered and acid-treated/untreated) show negligible activity towards decomposition (Table 1). However, the presence of metals substantially increases their decomposition activity. The AuPd catalysts with untreated carbon present the highest decomposition rate (36

and 49% for APO and AP respectively) whereas those with the acid-treated support show the lowest (10 and 15% for APO20 and AP20 respectively). This order exactly matches the selectivity obtained in the experiments of H_2O_2 synthesis and could be directly related to the presence of gold-rich alloy nanoparticles with sizes below 10 nm, as shown later.

Since the presence of gold-rich alloy nanoparticles seems to be important for the direct synthesis of water peroxide, the influence of the Au/Pd at. ratio during the preparation process was studied. AuPd bimetallic catalysts tested so far present 5 wt.% Au+Pd with a Au/Pd wt. ratio of 1. However, it cannot be assured that this Au/Pd ratio corresponds to the optimal composition. Therefore two more AuPd catalysts supported on ordered acid-treated carbons with different Au/Pd compositions (Au/Pd = 4 and Au/Pd = 0.25 wt. ratio) have also been prepared in the same way and tested in hydrogen peroxide formation. Figure 1b shows the hydrogen peroxide productivity after 10 and 90 min. In all cases, the catalyst with an Au/Pd wt ratio of 1 is the most efficient catalyst. On the other hand it has been observed that, apart from the Au/Pd composition, the reaction time plays an important role. Thus, after 90 min on line, most of the bimetallic catalysts perform better than pure Au or Pd catalysts and only the bimetallic Au-rich catalyst (4% in gold and 1% in palladium, APO20-B) presents after 10 min a H_2O_2 productivity lower than that obtained with only palladium. However, the production of H_2O_2 increases with the time on line for the Au-rich catalyst whereas for the palladium rich catalyst (APO20-C) the amount of hydrogen peroxide hardly varies after 10 min. Therefore it seems that the better selectivity to hydrogen peroxide could be again related to the presence of gold-rich alloy nanoparticles.

It should be highlighted that AuPd catalyst supported on ordered activated carbon showed to be reusable for three times, maintaining similar (slightly lower) productivity in all of the cycles. In addition, marginal metal leaching was detected during these experiments. However, when reuse tests were also carried out for the AuPd catalyst supported on the non-ordered activated carbon, a higher extent of metal leaching was observed, which could be related to a stronger metal-support interaction for bimetallic catalyst on the acid-treated support.

Table 1 shows the physical properties of the four carbon supports used in this study. In all cases, a very high surface area is measured, with non-ordered carbon (NORIT) (1210-1300 m^2 g^{-1}) showing a slightly higher surface area than those ordered (CMK-3) (975-1160 m^2 g^{-1}). No clear effect of the acid-treatment in the surface area is observed.

Both textural properties and nominal composition of the different catalysts used in this work are reported in Table 2. Metal containing carbons show surface areas in the range of 800 to 1000 m^2g^{-1}, which are lower values than those corresponding to carbon supports. The adsorption–desorption isotherms for AuPd bimetallic catalysts supported on ordered activated carbons are shown in Figure 2. The isotherms of the activated carbon supports are also plotted for comparative purposes. All the isotherms correspond to a type IV isotherm according to the IUPAC classification with a hysteresis loop due to capillary condensation in the mesopores. A uniform pore size distribution consistent with ordered CMK-3 materials with a mean pore size around 3 nm is obtained for all the samples, consistent with the reported properties of these materials [30]. As expected, a reduction in the porosity of the samples is attained after the incorporation of the noble metal nanoparticles. Noble metal nanoparticles supported either on the external surface

or inside the mesopores of the supports, can lead to partial pore blocking. In addition, it cannot be ruled out that a small amount of activated carbon porosity is destroyed during acid treatment, although specific surface area values are hardly decreased. Similar conclusions can be attained for the non-ordered activated carbons from the data shown in Tables 1 and 2.

To further understand the role of the surface chemistry of the carbon materials on the interaction of the metal and the support and consequently its effect on both nanoparticle size distribution and dispersion, the catalysts were calcined under an inert atmosphere, with the exhaust gases being analysed *in-situ* by a mass spectrometer. Figure 3A shows the CO_2 release profiles with respect to the temperature for the different carbon supports. It is observed that the acid pre-treatment of the CMK-3 support modifies the surface properties, compared to the untreated support, by the creation of oxygen surface sites for metal anchoring. The formation of carboxylic groups releasing CO_2 at low temperature is apparent [31]. On the other hand, Figure 3B shows the CO release profiles for the treated and untreated CMK-3 supports and their corresponding bimetallic catalysts. It can be observed that the amount of evolved CO also increases after acid pre-treatment of CMK-3, likely due to the formation of different CO evolving groups, such as lactones, anhydrides and phenols [31]. In order to confirm these surface differences, XPS in the O1s region for non-treated and pre-treated CMK-3 supports have been also conducted and are shown in Figure 3C. The O 1s spectrum, in both samples, showed an asymmetric peak in which we could resolve (after Gaussian fitting) two components: A more intense Gaussian-like lobe, centered around 532.9 eV and a second one appearing at energies around 530.6 eV. These components may be identified to the presence of O-C-O and C=O in our samples, respectively. The intensity of the O

1s spectra showed in the figure has been normalized to the C 1s intensity spectra leading to comparable results for both catalysts, regardless the nature of the carbon support. These results indicated that the accessible surface of ordered carbon samples detected by XPS seemed to remain basically unaltered after treatment. Therefore, it could be tentatively assumed that oxygen surface groups could be mainly created in the inner porosity, later favouring the encapsulation of nanoparticles. Accordingly, it should be noted that whilst both the amount and the profile of the evolved CO and CO_2 are comparable for the ordered CMK-3 support and its corresponding bimetallic catalysts (APO), a remarkable decrease in the amount of surface oxygen groups is observed for the AuPd catalyst supported on acid-treated ordered support (APO20) when compared to the support itself (O20). These results again suggest that the oxygen surface sites are created in the inner porosity after acid treatment. These sites could favour the interaction of noble metal precursors with the activated carbon surface during the impregnation step, leading to the formation of very small metal nanoparticles (~2-3 nm) which, when incorporated to the porous structure, limited their further growth through encapsulation [32]. Then, it can be concluded that the acid pre-treatment of activated carbons seemed to favour both small size metal nanoparticles and their dispersion.

The nature of these bimetallic nanoparticles was also studied by XPS analysis. Figure 4 shows the Pd 3d and Au 4f spectra measured by XPS of bimetallic nanoparticles prepared over acid-treated mesoporous ordered and non-ordered carbon supports (APO20 and AP20). The binding energies of the Pd 3d5/2 and the Au 4f7/2 are 335.4 ± 0.2 eV and 83.6 ± 0.2 eV. When these values are compared to those expected for either metallic Pd (335.0 eV) [35] or Au (83.95 eV) [36], a small but non-negligible shift (~0.3 eV) can be detected, which indicates changes from Pd to Au core levels. These

results suggest that some charge transfer occurs between Au and Pd, with Au acting as a donor, which is indicative of the nanoparticle bonding nature. In each of these XPS spectra, a unique spin-orbit doublet has been resolved corresponding to the Pd 3d and Au 4f core-levels with a characteristic spin-orbit splitting of 5.3 eV and 3.8, respectively, and with an intensity ratio between the two peaks of the doublet given by the (2J + 1) degeneracy of the states. To deepen the analysis of these spectra, a Gaussian fitting procedure of the doublets was performed after subtracting the background. By this fitting procedure, similar values of the full width at half the maximum of the core-level peaks are obtained in all the studied samples. An estimate of the Pd/Au at. ratio can be obtained by means of the integrated intensity of the XPS peaks and using empirical atomic sensitivity factors [34]. Pd/Au wt. ratios for the APO20 and AP20 catalysts are around 1.2 and 2.3, respectively. Therefore, surface Pd/Au wt. ratios are higher than those obtained in the bulk EDX analysis which are close to 1. This fact could be related to an enrichment of palladium at the surface of the nanoparticles, as previously reported [21]. XPS experiments were also used to determine the accessibility of the bimetallic nanoparticles in the pores, as XPS is sensitive to the amount of non-covered surface particles and covered particles in a short depth range (the mean-free path of photoelectrons is typically around 2 nm). Thus, the metal/C ratio was determined by XPS for those bimetallic catalysts supported on both ordered and non-ordered carbons pre-treated with acid. Whilst Au/C and Pd/C wt. ratios are 0.0036 and 0.0030, respectively, for APO20, these values are considerably higher in the case of the AP20 catalyst, 0.0042 and 0.010 for the Au/C and the Pd/C wt. ratios, respectively. The lower amount of surface metals detected in the case of nanoparticles supported on acid-treated ordered carbons could be linked to the fact that a large proportion of the metal

alloy nanoparticles could be encapsulated inside the inner porosity of the carbon support, and then, they cannot be detected by XPS.

The formation of the alloy nanoparticles with noticeable catalytic effects towards hydrogen peroxide formation can also be corroborated by the XRD patterns. XRD profiles corresponding to catalysts prepared over acid-treated CMK-3 ordered support are plotted in Figure 5. The Pd-only catalyst show a diffraction peak at *ca*. 40º corresponding to metallic palladium while reflection peaks are shown at 38.2° and 44.3° corresponding to metallic gold are observed for the Au-only catalyst, however, for the Au–Pd catalysts the reflection peaks corresponding to Au shifts to higher angles in comparison with the Au only catalysts, which is again an indication of alloy formation.

Nanoparticle alloy formation and encapsulation was studied by TEM analysis. Figure 6 shows representative TEM images and the metal particles' size distributions of monometallic gold and palladium catalysts supported on treated ordered carbons (PO20 and AO20 respectively). As can be seen in the TEM images of the AO20 catalyst (Fig. 6a,b), Au particles are relatively large, mostly in the range of 15-40 nm with the presence of bigger agglomerations (> 60 nm). Additionally, gold is not uniformly distributed on the surface of the carbon, presenting zones without gold and others with a relatively high concentration of gold particles. Most of the gold is located on the outer carbon surface, with no presence inside the pores of the ordered structure. On the other hand, in the case of the monometallic palladium catalyst (PO20), Pd particles are small, with more than half of particles smaller than 5 nm with less than 10% being larger than 10 nm (Fig. 6f), and spread uniformly on the surface of the carbon (Fig. 6d,e). A careful analysis of the location of the particles reveals that palladium particles are both on the

surface of the carbon and also inside the pores, in contrast with that observed in the gold catalyst. The size of the metal nanoparticles is strongly related to the catalytic activity, being the hydrogen peroxide productivity indirectly proportional to the particle size, which could partly explain the differences found in the activity of these monometallic catalysts. Additionally, and aligned with previous observations, gold nanoparticles become practically inactive when their size is above ~20 nm.

Figure 7 shows TEM images and particle size histograms of bimetallic AuPd catalysts supported on an ordered carbon and on a non-ordered commercial carbon, in both cases the support had been previously treated with nitric acid. For Au-Pd supported on the non-ordered carbon catalyst (AP20), a unimodal particle size distribution centred at 7 nm, with most particles in the 5-12 nm range (Fig. 7d) can be seen. However, in the AuPd sample over the ordered carbon (APO20), a remarkably lower particle size is observed with around 80% of the particles smaller than 3 nm (Fig. 7b), many of them located inside the pores, as anticipated by XPS analysis. The influence of the acid pre-treatment of the support over the nanoparticle size distribution and location has been previously shown [27]. Briefly, pre-treatment of the carbon support with nitric acid strongly affects not only the metal particle size but also its location. Thus, when the ordered CMK-3 carbon support is not acid-treated, the mean particle size is remarkably higher (9.9 nm vs 2.7 nm) and the amount of particles inside the pores is drastically reduced (less than 10%). Likewise, if the non-ordered NORIT carbon is not acid-treated the same effect is observed, as the mean particle size in that case is of *ca.* 14.4 nm, considerable higher than for the treated sample, *ca.* 7.0 nm.

As previously mentioned, EDX-mapping analysis was also conducted to determine the composition of the bimetallic AuPd nanoparticles. Bright field TEM images and EDX-mapping of the selected area were conducted for bimetallic catalysts and data corresponding to the most efficient catalyst, AuPd supported on acid-treated CMK-3 carbon (APO20), are depicted in Figure 7a. As can be seen in the elemental map, Au and Pd appear in the same positions, suggesting the formation of an alloy, which is aligned with the observed synergetic catalytic effect and XRD and XPS characterization data. We have previously shown by quantitative EDX mapping that the composition of the AuPd particles is not homogeneous and its distribution depends on the particle size, support used and acid pre-treatment [27]. The metal distribution in the particles in the size range of 5 to 10 nm has been used for comparison. The composition of particles below 5 nm cannot be properly determined with the available equipment. Pre-treatment of the support with nitric acid seems to increase the presence of gold in small nanoparticles as the composition of the particles in this size range for the AuPd catalyst supported on untreated and non-ordered carbon (AP) is remarkably richer in palladium (Au/Pd=17/83) than that of the same catalyst pre-treated with acid (AP20, Au/Pd=39/61). Moreover, higher gold enrichment is obtained by the use of the ordered CMK-3 pre-treated support (APO20), with the particles in the 5 to 10 nm range being richer in gold (Au/Pd=56/44). However, it is worth to point out that although these nanoparticles are not homogeneous and palladium-rich surfaces are always present, according to XPS data, a higher gold concentration is observed in the surface of the smallest particles.

Further structural characterisation of Au, Pd and bimetallic Au-Pd nanoparticles was achieved by using high resolution TEM and selected area electron diffraction (SAED).

Figure 8 shows HRTEM images of selected particles and their corresponding Fast Fourier Transform (FFT). It is important to highlight that the size of Au nanoparticle selected (~12 nm) is twice as big as the Pd nanoparticle selected (~5 nm). The well-defined spots of the electron diffraction patterns of the selected individual Au and Pd nanoparticles show the single crystal properties. Moreover, a careful analysis of HRTEM images and their corresponding FFTs showed that the measured interplanar distance from fringes are about 2.356 Å and 2.286 Å attributable to the (111) family planes of cubic phase structure of Au and Pd, respectively. The measured a-lattice parameters of metallic Au and metallic Pd are 4.087 Å and 3.960 Å, respectively, aligned with the JCPDS database for the metallic Au and Pd in their respective face-centred cubic structure with space group. In the case of the bimetallic Au-Pd, the FFT showed diffused spots arrange in a single ring with the same radius from the centre (transmitted beam spot) due to the loose structure of the single crystal quality resulting in the polycrystalline property of the selected AuPd nanoparticles. The measured interplanar distance from spacing fringes and from spots in FFTs pattern are in the order of 2.334 Å which could be attributed to (111) family plane of cubic phase structure of Au. The measured a-lattice parameter of AuPd sample (4.043 Å) shows a lower value compared with the Au metallic one. This result is in concordance with the XRD pattern result that showed a shift of (111) Au diffraction peak to higher 2θ angle. Both the decrease in the a-lattice parameter of Au to lower values and the X-ray diffraction peak shift are evidence of the incorporation of Pd in the Au lattice which is likely to be responsible for the synergetic catalytic effect towards the direct synthesis of hydrogen peroxide.

Figure 9 shows TEM images for AuPd catalysts on the ordered pre-treated carbons which are rich in palladium (a,b) or rich in gold (c,d). The AuPd catalyst rich in palladium (APO20-C) shows two very different zones. First, a minor area where the carbon is not fully ordered with large particles either bimetallic (the largest ones) or containing only Pd (smaller but still large). EDX mapping was used to determine the nanoparticle composition (Fig. 9a). Second, a prevalent area (Fig. 9b), corresponding to the most ordered structure, where small bimetallic particles of mainly 2-4 nm can be observed, many of them being incorporated inside the pores of the ordered carbon. No palladium particles have been detected in this second area. Figures 8c and 8d show TEM images for the AuPd catalyst rich in gold (APO20-B). The characteristics of this catalyst are remarkably different to those of the other AuPd catalysts since a larger size of these particles, most of them over 10 nm and some of them exceeding 60 nm, is observed. However, only bimetallic particles have been observed regardless of the nanoparticle size. Therefore, in contrast with the other bimetallic catalysts supported on ordered treated carbon, no nanoparticles have been encapsulated inside the pores.

Therefore, the composition of the bimetallic catalysts supported on ordered and pre-treated carbons has demonstrated to be very important in order to promote the direct synthesis of hydrogen peroxide. Thus, the most efficient catalyst tested is that with the equivalent amount of gold and palladium (APO20). We relate the best performance of APO20 with the presence of very small AuPd nanoparticles with gold enrichment, which can be formed throughout their encapsulation inside the mesopores. This encapsulation process is facilitated by the presence of oxygen surface groups created after acid pre-treatment of the carbon support. Similarly to our results, Tiruvalam et al. [37] showed the positive effect of small particles on carbon, but they observed the

opposite trend if the support was titania, relating this behaviour to the exceptionally high activities of small particles in AuPd/TiO_2 catalysts for the hydrogenation of H_2O_2.

Conversely, in the Au-rich catalyst (APO20-B) the bimetallic nanoparticles formed are extremely large, this affecting the catalytic performance. The formation of large particles must be due to the trend of gold for forming large particles (see Figure 2a) when a simple impregnation method, as the one used in the present article, is employed. On the other hand, if a higher amount of palladium is employed (APO20-C) small nanoparticles are also created but they are richer in palladium, which are supposed to be related to a poorer selectivity to hydrogen peroxide.

Finally, it should be commented that the improvement obtained in the production of water peroxide for the AuPd catalysts supported on acid-treated ordered carbon is not as drastic as the particle size could suggest, as the pre-treated ordered catalyst (APO20), with very tiny particles, is only a 53% more active than the pre-treated unordered catalyst (AP20). This not so large difference can be related with the structure of the catalyst as in the ordered catalyst a significant part of the AuPd particles could not be accessible as they are covered up by the ordered carbon, as suggested by the XPS and microscopy study. On the other hand, it must be noted that the acid pre-treatment may remove trace metal impurities from carbons which may be responsible for H_2O_2 degradation by hydrogenation in the presence of H_2. However, conversely to other carbons prepared from coal or biomass, the supports prepared in the present paper were lab-made carbons produced in the lab with high purity commercial chemicals (see Experimental section). For these carbons the amount of impurities is very low. In fact, no ashes were detected after static calcination of 1 gram of ordered carbon at 850ºC. In

any case, a positive role of the acid pre-treatment for removing impurities cannot be completely ruled out.

Conclusions

Ordered mesoporous carbons with a CMK-3 structure previously treated with acid are excellent supports for highly dispersed bimetallic gold-palladium nanoparticles (2-3 nm) compared to non-ordered mesoporous carbon, related to the alloy nanoparticle encapsulation in the former case. The pre-treatment of both of the supports with acid enhances the metal dispersion and the gold enrichment of the smaller nanoparticles. In fact, the incorporation of palladium into the gold lattice is observed by XPS and XRD. As a consequence, the resulting catalysts present high productivities towards the direct synthesis of hydrogen peroxide with little decomposition activity and consequently high hydrogen selectivities. It must be mentioned that the AuPd composition determines the catalytic performance and in this study the optimal composition corresponds to an Au/Pd wt. ratio of 1.

Acknowledgments

The authors would like to thank MINECO and FEDER (project CTQ2012-37984-C02-01 and CTQ2012-37925-C03-02 Spain) and EPSRC (grant number EP/K016334/1, UK) for funding. B.P. acknowledges the Spanish Ministry of Education for her scholarship (FPU grant AP2009-3544).

References

1. J. M. Campos-Martin, G. Blanck-Brieva and J. L. G. Fierro, Angew. Chem., Int. Ed., 45 (2006) 6962-6984.

2. H.-J. Reidl, G. Pfleiderer (I.G. Farbenindustrie AG), US Patent 2,158,525 (1939).

3. C. Samanta, Applied Catalysis A: General 350 (2008) 133–149.

4. H. Henkel, W. Weber (Henkel & CIE), US Patent 1,108,752 (1914).

5. V. R. Choudhary, C. Samanta and A. G. Gaikwad, Chem. Commun. (2004) 2054.

6. V. R. Choudhary and C. Samanta, J. Catal. 238 (2006) 28.

7. V.R. Choudhary, A.G. Gaikwad, S.D. Sansare, Angew Chem. Int. Ed. 40 (2001) 1176.

8. G. Bernardotto, F. Menegazzo, F. Pinna, M. Signoretto, G. Cruciani and G. Strukul, Appl. Catal., A, , 358 (2009) 129.

9. V.R. Choudhary, P. Jana, Applied Catalysis A: General 352 (2009) 35-42

10. C. Samanta, V.R. Choudhary, Appl. Catal. A: Gen. 330 (2007) 23.

11. C. Burato, P. Centomo, M. Rizzoli, A. Biffis, S. Campestrini, B. Corain, Adv. Synth. Catal. 348 (2006) 255.

12. S. Abate, M. Freni, R. Arrigo, M.E. Schuster, S. Perathoner, G. Centi, ChemCatChem 5 (2013) 1899-1905

13. P. Landon, P.J. Papworth, C.J. Kiely, G.J. Hutchings, Chem. Commun. (2002) 2058.

14. J.K. Edwards, J. Pritchard, M. Piccinini, G. Shaw, Q. He, A. Carley, C.J. Kiely, G.J. Hutchings, J. Catal. 292 (2012) 227–238

15. Y.-F. Han, Z. Zhong, K. Ramesh, F. Chen, L. Chen, T. White, Q. Tay, S. Nurbaya, Z.Wang, J. Phys. Chem. C 111 (2007) 8410.

16. T. Ishihara, Y. Hata, Y. Nomura, K. Kaneko, H. Matsumoto, Chem. Lett. 36 (2007) 878.

17. P.P. Olivera, E.M. Patrito, H. Sellers, Surf. Sci. 313 (1994) 25.

18. M. Okumura, Y. Kitagawa, K. Yamagcuhi, T. Akita, S. Tsubota and M. Haruta, Chem. Lett. 32 (2003) 822.

19. S. Chinta, T.V. Choudhary, L.L. Daemen, J. Eckert, D.W. Goodman, J.Am. Chem. Soc. 126 (2004) 38.

20. P. Landon, P.J. Collier, A.F. Carley, D. Chadwick, A.J. Papworth, A. Burrows, C.J. Kiely, G.J. Hutchings, Phys. Chem. Chem. Phys. 5 (2003) 1917.

21. J. K. Edwards, A. Thomas, B. Solsona, P. Landon, A. F. Carley and G. Hutchings, Catal. Today 122 (2007) 397.

22. J.K. Edwards, B.E. Solsona, P. Landon, A.F. Carley, A. Herzing, C.J. Kiely, G.J. Hutchings, J. Catal. 236 (2005) 69.

23. B.E. Solsona, J. K. Edwards, P. Landon, A.F. Carley, A. Herzing, C.J. Kiely and G.J. Hutchings, Chem. Mater. 18 (2006) 2689-2695.

24. J.K. Edwards, B. Solsona, P. Landon, A.F. Carley, A. Herzing, M. Watanabe, C.J. Kiely, G.J. Hutchings, J. Mater. Chem. 15 (2005) 4595.

25. J. K. Edwards, B. Solsona, E. Ntainjua N, A. F. Carley, A. A. Herzing, C. J. Kiely and G. J. Hutchings, Science 323 (2009) 1037.

26. J. K. Edwards, E. Ntainjua N, A. F. Carley, A. A. Herzing, C. J. Kiely and G. J. Hutchings, Angew. Chem., Int. Ed. 48 (2009) 8512.

27. T.Garcıa, R. Murillo, S. Agouram, A. Dejoz, M.J. Lazaro, L. Torrente-Murciano and B. Solsona, Chem. Commun., 48 (2012) 5316–5318.

28. S. H. Joo, S. J. Choi, I. Oh, J. Kwak, Z. Liu, O. Terasaki and R. Ryoo, Nature 412 (2001) 169.

29. T. García, R. Murillo, D. Cazorla-Amorós, A. M. Mastral, A. Linares-Solano, Carbon 42 (2004) 1683.

30. S. Jun, S. H. Joo, R. Ryoo, M. Kruk, M. Jaroniec, Z. Liu, T. Ohsuna, O. Terasaki, J. Am. Chem. Soc. 122 (2000) 10712.

31. J.L. Figueiredo, M.F.R. Pereira, M.M.A. Freitas, J.J.M. Órfão, Carbon 37 (9), (1999) 1379-1389.

32. S. Abate, G. Centi, S. Melada, S. Perathoner, F. Pinna, G. Strukul, Catal. Today, 104 (2005) 323.

33. H. C. Ham, G. S. Hwang, J. Han, S. W. Nam and T. H. Lim, J. Phys. Chem. C, , 113 (2009) 12943.

34. C.D. Wagner, L.E. Davis, M.V. Zeller, J.A. Taylor, R.M. Raymond, L.H. Gale, Surf. Interface Anal. 3 (1981) 211.

35. C.J. Jenks, S.-L. Chang, J.W. Anderegg, P.A. Thiel, D.W. Lynch, Phys. Rev. B 54, (1996) 6301.

36. M.P. Seah, I.S. Gilmore, G. Beamson, Surf. Interface Anal. 26, (1998) 642

37. R. C. Tiruvalam, J. C. Pritchard, N. Dimitratos, J. A. Lopez-Sanchez, J. K. Edwards, A. F. Carley, G. J. Hutchings, C. J. Kiely, Faraday Discussions, 152 (2011) 63.

Caption of figures

Figure 1. a) Evolution of the H_2O_2 concentration with the time line for AuPd/carbon catalysts in the direct synthesis of hydrogen peroxide from molecular oxygen and hydrogen. b) Influence of the Au/Pd composition in catalysts supported on pre-treated ordered carbon over the productivity to H_2O_2 after 10 or 90 min on line. The reaction conditions are in the text.

Figure 2. Adsorption–desorption isotherms for the ordered carbon supports and for the AuPd catalysts supported on ordered activated carbons.

Figure 3. TPD profiles of CO_2 (5A) and TPD profiles of CO (5B) of the activated carbon supports and the AuPd catalysts supported on ordered activated carbons. Fig. 3C shows the XPS on the O1s region for untreated and pre-treated carbon supports.

Figure 4. XPS spectra of the (a) Pd 3d and (b) Au 4f core levels measured in NPs prepared over ordered-mesoporous (APO20) and non-ordered carbon substrates (AO20 catalyst). The spectra acquired in different samples have been normalised to background intensity, for the ease of comparison. Note the presence of oxidized Ca at 348.0 eV.

Figure 5. XRD patterns of Au (AO20), Pd (PO20) and AuPd/carbon (APO20) catalysts. Note: In all cases the supports previously pre-treated with nitric acid.

Figure 6. Representative TEM micrographs for Au/carbon, AO20 catalyst (a,b) and Pd/carbon, PO20 catalyst (d,e). The corresponding histograms of AO20 (c) and PO20 (f) are also shown. Note: Both supports previously pre-treated with nitric acid.

Figure 7. Representative TEM micrographs for AuPd/ordered carbon, APO20 (a) and for AuPd/ non-ordered carbon, AP20 catalyst (c). The corresponding histograms of APO20 (b) and AP20 (d) are also shown. Note: Both supports previously pre-treated with nitric acid.

Figure 8. High Resolution TEM images and FFT of selected nanoparticles of Au, Pd and AuPd supported on ordered mesoporous carbon in AO20, PO20 and APO20 catalysts. Note: In all cases the supports previously pre-treated with nitric acid.

Figure 9. Representative TEM micrographs for AuPd/ordered pre-treated carbon rich in Pd, APO20-C (a,b) and rich in Au, APO20-B (c,d). EDX mapping are found as insets in a and c.

Figure 1

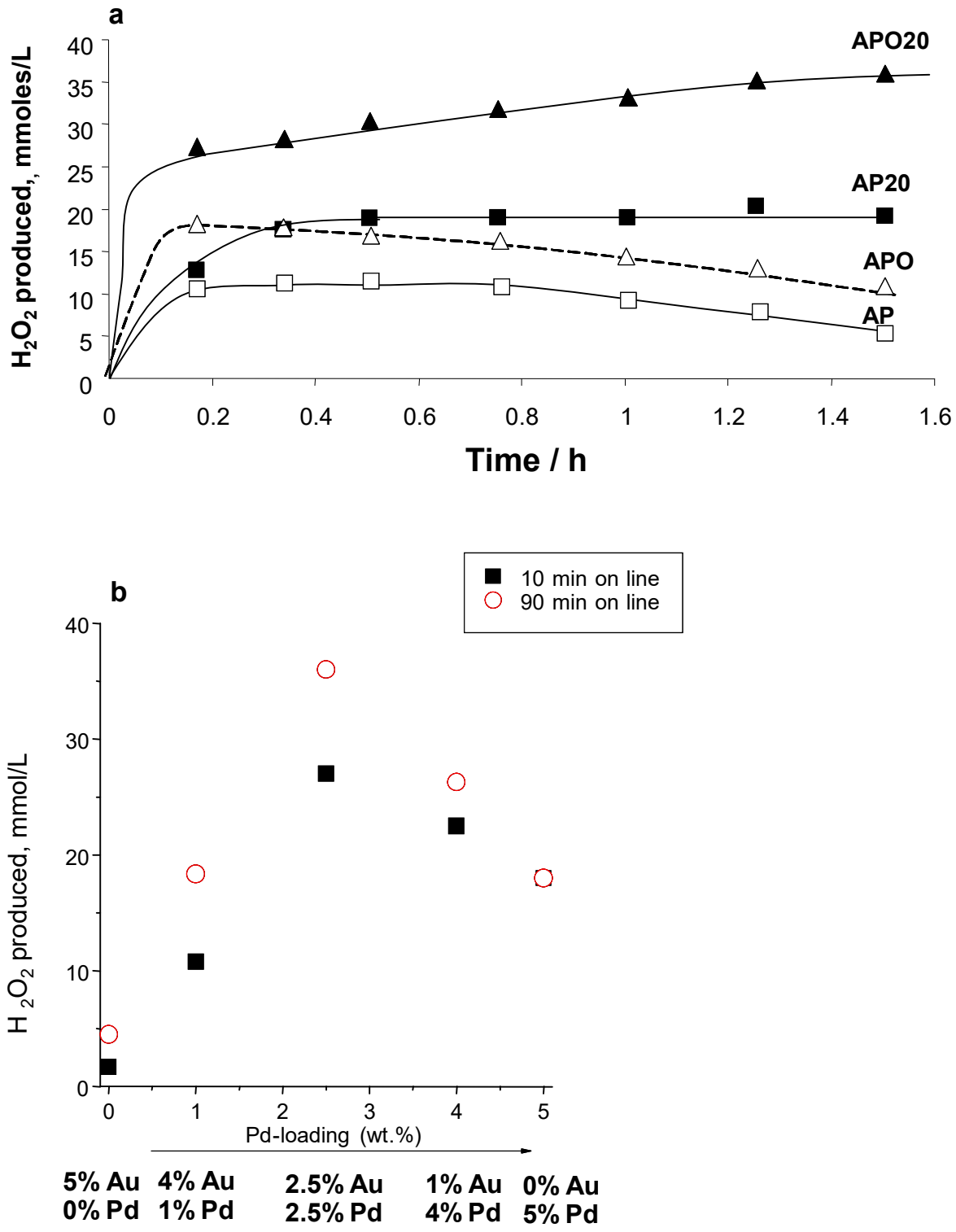
a
APO20
AP20
APO
AP
H_2O_2 produced, mmoles/L
Time / h
b
10 min on line
90 min on line
H_2O_2 produced, mmol/L
Pd-loading (wt.%)
5% Au 0% Pd
4% Au 1% Pd
2.5% Au 2.5% Pd
1% Au 4% Pd
0% Au 5% Pd

Figure 2

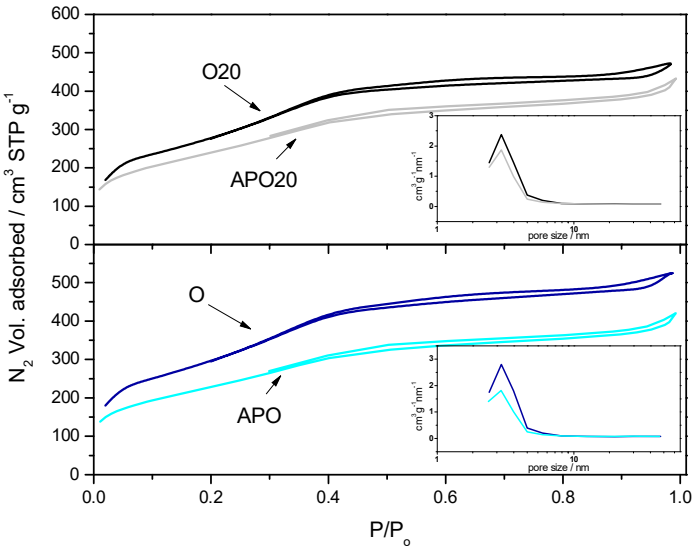
O20
APO20
O
APO
N2 Vol. adsorbed / cm3 STP g-1
P/Po
pore size / nm
cm3g-1nm-1

Figure 3

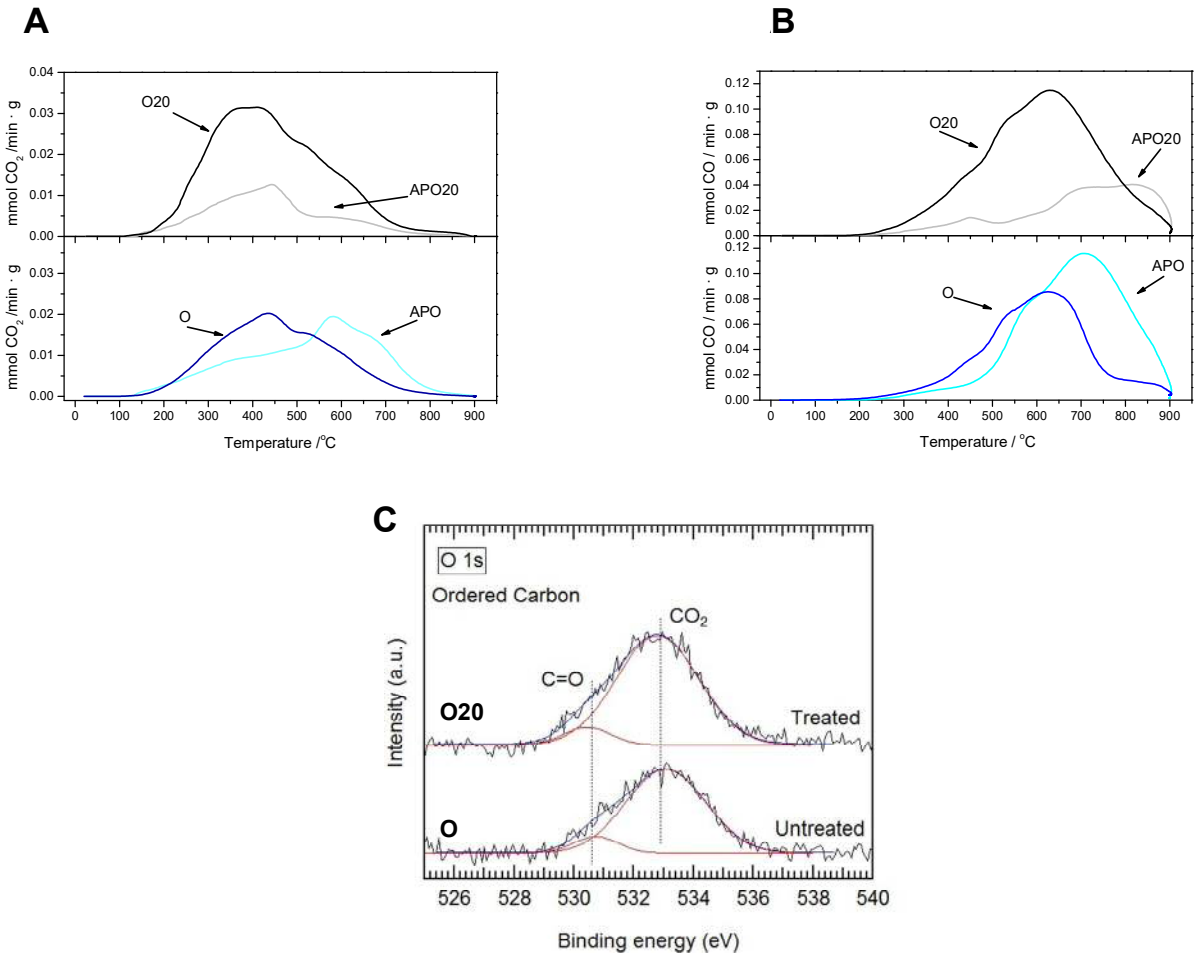
A
B
C
O20
APO20
O
APO
mmol CO2 /min · g
mmol CO / min · g
Temperature /°C
O 1s
Ordered Carbon
CO2
C=O
Treated
Untreated
Intensity (a.u.)
Binding energy (eV)

Figure 4

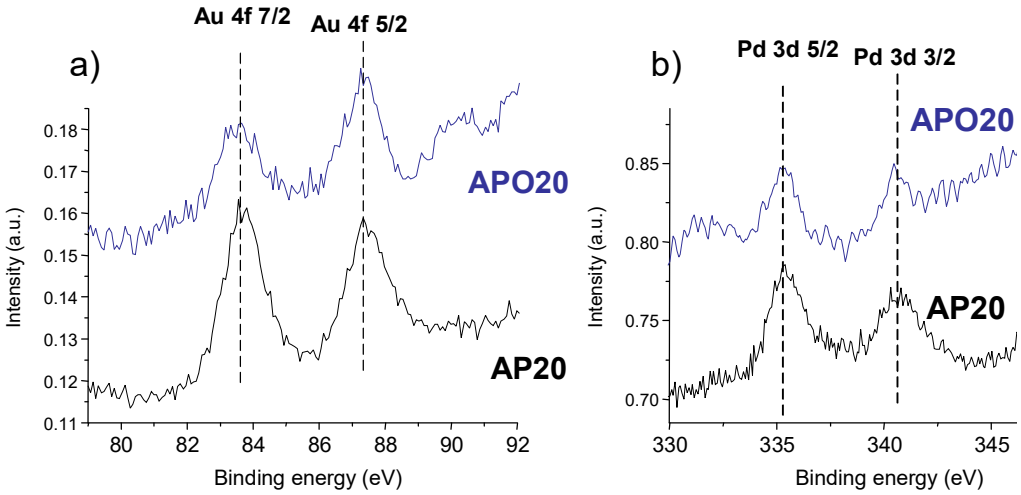
a)
Au 4f 7/2
Au 4f 5/2
APO20
AP20
Intensity (a.u.)
Binding energy (eV)
b)
Pd 3d 5/2
Pd 3d 3/2
APO20
AP20
Intensity (a.u.)
Binding energy (eV)

Figure 5

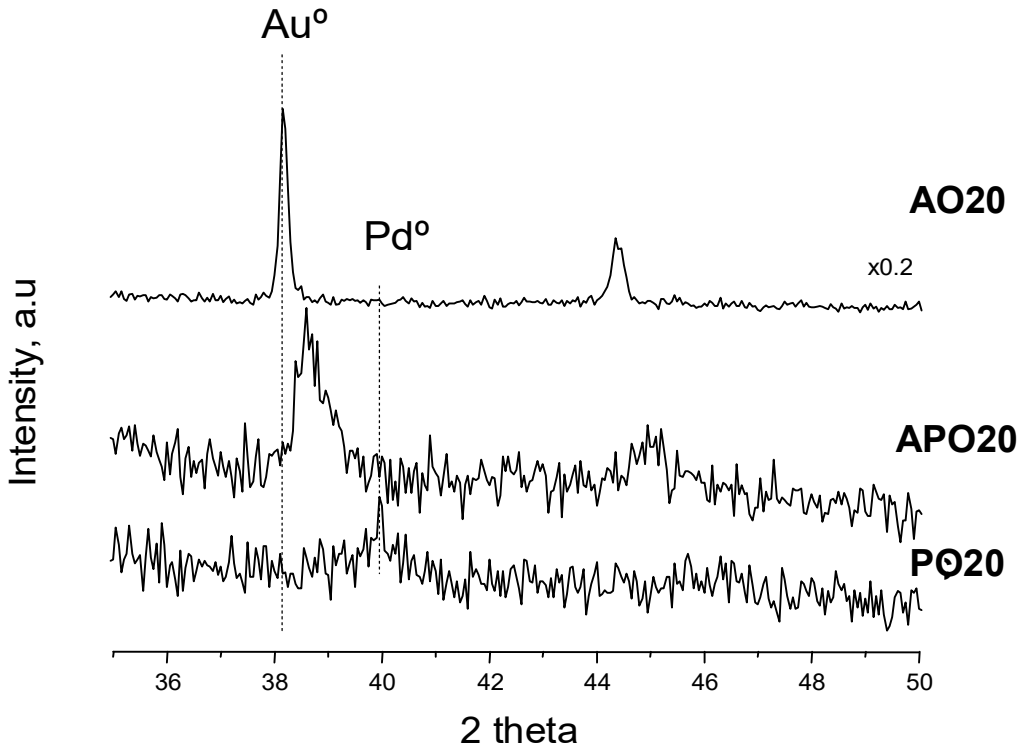
Au°
Pd°
AO20
x0.2
APO20
PO20
Intensity, a.u
36
38
40
42
44
46
48
50
2 theta

Figure 6

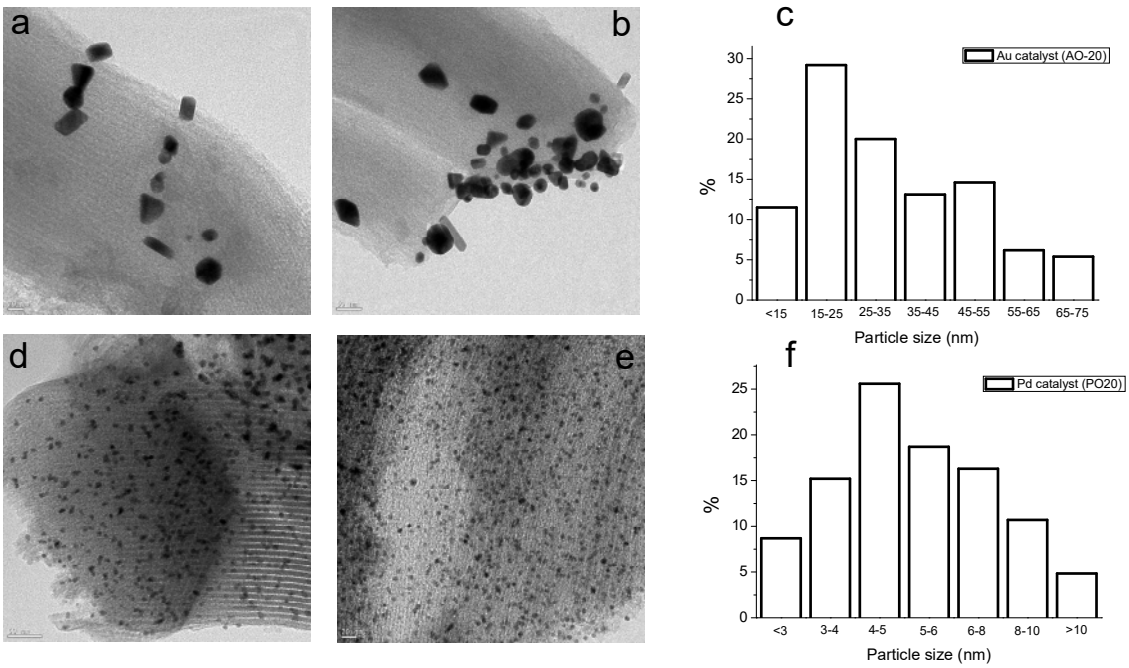
a
b
c
Au catalyst (AO-20)
%
Particle size (nm)
<15
15-25
25-35
35-45
45-55
55-65
65-75
d
e
f
Pd catalyst (PO20)
%
Particle size (nm)
<3
3-4
4-5
5-6
6-8
8-10
>10

Figure 7

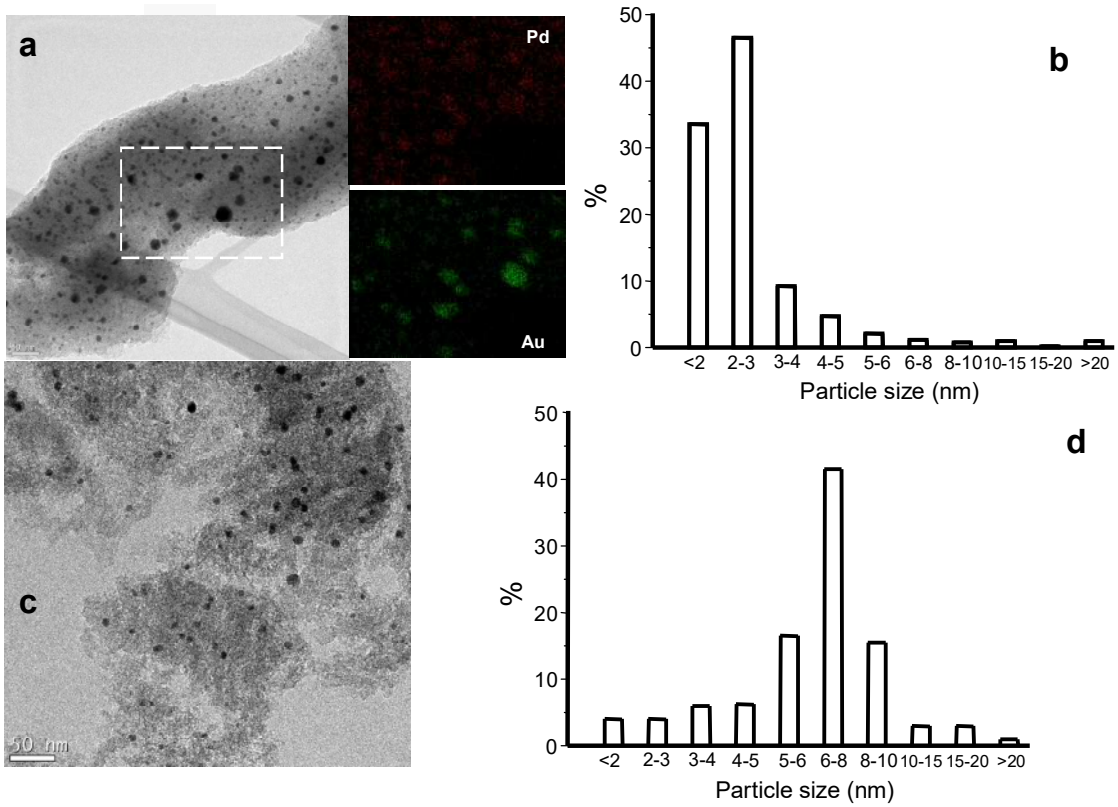
a
Pd
Au
b
%
Particle size (nm)
<2
2-3
3-4
4-5
5-6
6-8
8-10
10-15
15-20
>20
c
50 nm
d

Figure 8

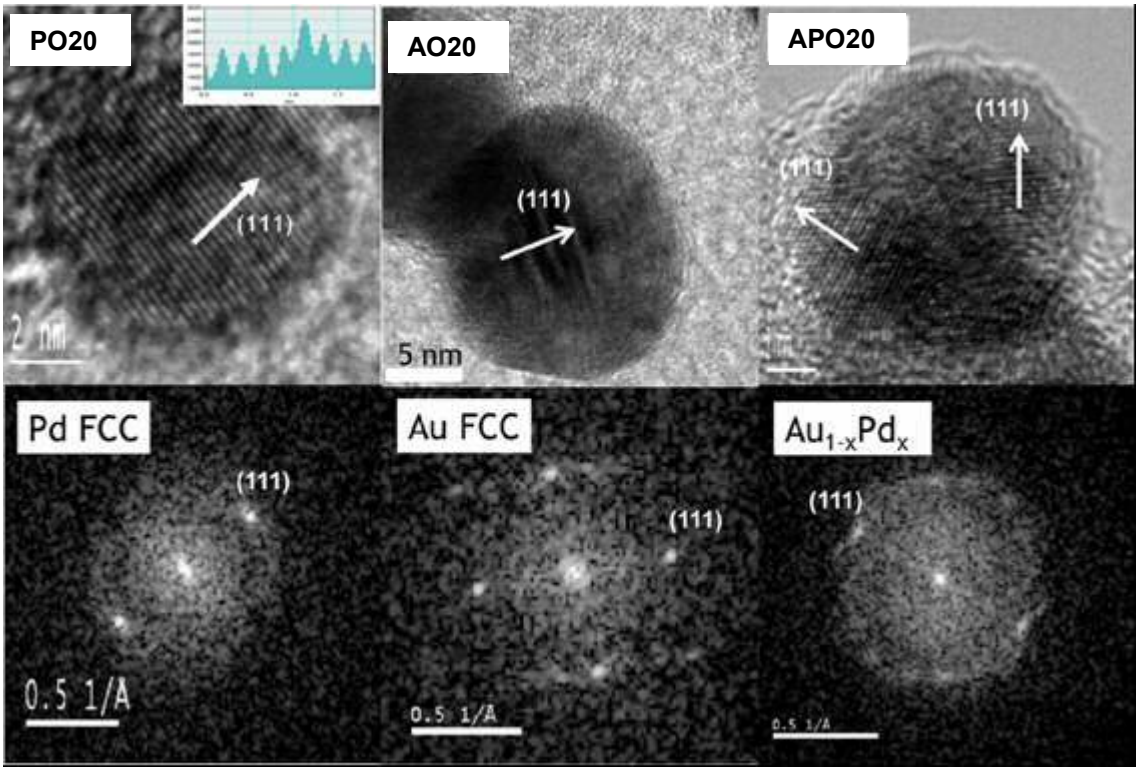
PO20
(111)
2 nm
AO20
(111)
5 nm
APO20
(111)
(111)
Pd FCC
(111)
0.5 1/A
Au FCC
(111)
0.5 1/A
Au1-xPdx
(111)
0.5 1/A

Figure 9

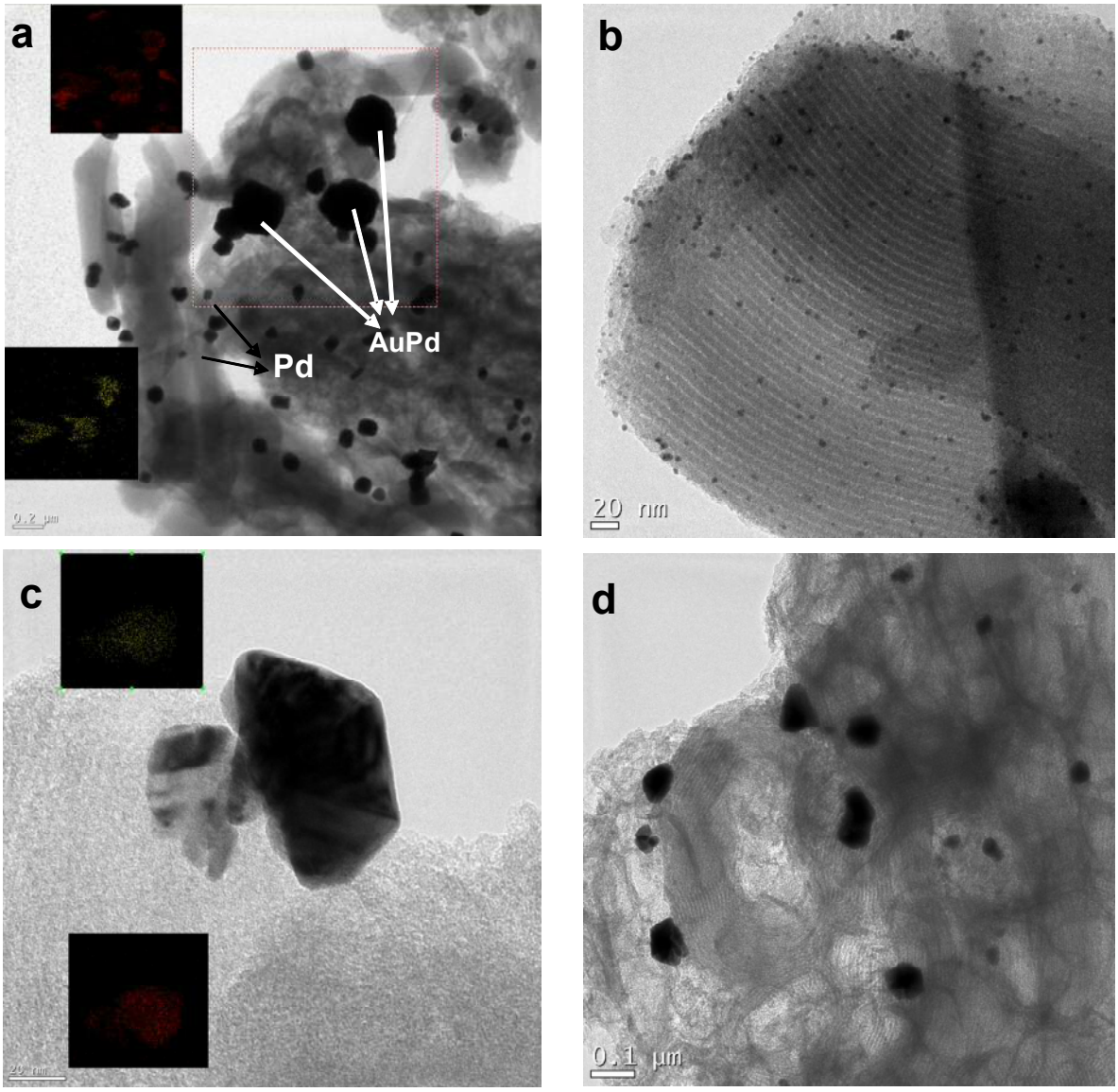

Table 1. Physical and catalytic properties of the carbon supports.

Carbon support	**Pre-treatment**	**Catalytic performance**		S_{BET}	$V_{mesopore}$	d_{pore}
		H_2O_2 Synthesis[a]	**H_2O_2 Decomposition[b]**	**[m^2 g^{-1}][c]**	**[cm^3g-1][d]**	**[nm][d]**
NORIT (non ordered)	HNO_3 treated	<0.1	0	1300	0.44	4.6
NORIT (non ordered)	Untreated	<0.1	0	1211	0.46	4.6
CMK-3 (ordered)	Untreated	<0.1	0	1163	0.80	3.3
CMK-3 (ordered)	HNO_3 treated	<0.1	0	975	0.70	3.4

[a] Productivity to H_2O_2 after 60 min, Reaction conditions in text;

[b] Decomposition of H_2O_2 after 60 min, reaction conditions in text;

[c] BET surface area from the N_2 adsorption isotherm;

[d] Calculated using the BJH method to the desorption branch of the N_2 adsorption isotherm

Table 2. Textural properties obtained from N_2 adsorption isotherm data for Au, Pd and AuPd catalysts.

Catalysts[a]	Metal loading, wt.%		Carbon Treatment	Order	S_{BET} [m^2 g^{-1}][b]	Vmesopore [cm^3g-1][c]	dpore [nm][c]
	Au	Pd					
AO20	5.0	0	2 wt.% HNO_3	Yes, CMK-3	815	0.54	3.5
AP	2.5	2.5	Not treated	No	980	0.53	4.5
AP20	2.5	2.5	2 wt.% HNO_3	No	897	0.49	4.6
APO	2.5	2.5	Not treated	Yes, CMK-3	822	0.54	3.4
APO20	2.5	2.5	2 wt.% HNO_3	Yes, CMK-3	860	0.54	3.4
APO20-B	4.0	1.0	2 wt.% HNO_3	Yes, CMK-3	847	0.54	3.5
APO20-C	1.0	4.0	2 wt.% HNO_3	Yes, CMK-3	862	0.54	3.4
PO20	0	5.0	2 wt.% HNO_3	Yes, CMK-3	854	0.54	3.4

[a] Nomenclature of the catalysts.

[b] Surface area from the N_2 adsorption isotherm using BET method

[c] Calculated using the BJH method to the desorption branch of the N_2 adsorption isotherm

Table 3. Catalytic characteristics of 2.5%wtAu-2.5%wtPd / carbon catalysts in the direct synthesis of H_2O_2 from H_2 and O_2 and in the H_2O_2 decomposition.

Catalyst [a]	**Synthesis of H_2O_2**					**H_2O_2 decomposition**[d]
	Production of H_2O_2 [a]			**Activity**[b]	**Selectivity to H_2O_2**[c]	
	10 min	**60 min**	**90 min**			
AO	n.a.	4.3	n.a	n.a	n.a	n.a
AO20	1.7	4.2	4.5	n.a	n.a	n.a
AP	11	11	5.6	34	32	49
AP20	13	19	19	21	89	15
APO	18	15	11	37	40	36
APO20	27	32	36	32	>99	10
APO20-B	11	16	19	n.a	n.a	n.a
APO20-C	23	26	26	n.a	n.a	n.a
PO	n.a.	10	n.a	n.a	n.a	n.a
PO20	18	21	18	n.a	n.a	n.a

[a] H_2O_2 produced after 10, 60 and 90 min expressed as mmol of H_2O_2/L. Reaction conditions in text;
[b] Activity after 60 min expressed as mmol of H_2 reacted/(l.h);
[c] Selectivity to H_2O_2 referred to H_2 after 60 min;
[d] Decomposition of H_2O_2 after 60 min. Reaction conditions in text.